Pergamon

*Journal of Structural Geology*, Vol. 18, No. 4, pp. 461 to 474, 1996
Published by Elsevier Science Ltd

0191-8141/96 $15.00+0.00

0191-8141(95)00099-2

# The deformation of multilayers by layer-normal compression; an experimental investigation

T. W. KIDAN and J. W. COSGROVE

Department of Geology, Imperial College, London SW7 2BP, U.K.

(*Received* 12 *July* 1993; *accepted in revised form* 6 *August* 1995)

**Abstract**—In this paper, experiments are described which were carried out to investigate the initiation and amplification of structures which form when a multilayer is compressed normal to the layering. The multilayers were made up of either putty or paraffin wax and an attempt is made to relate the structures that form to those predicted by the various theories which consider the deformation of either a single layer, a multilayer or an anisotropic material when compressed normal or at a high angle to the layering or fabric.

The experiments give an insight into the temporal and spatial relationships between the various types of structures that form by showing clearly how the initiation and growth of one type of structure such as a boudin can provide the local perturbation necessary for the initiation of other structures such as internal pinch-and-swell structures or normal kink bands.

## INTRODUCTION

A variety of structures can form when a complex geological multilayer (i.e. one made up of different layers each with its own thickness and competence) is compressed normal or at a high angle to the layering. They can be divided into two groups, those that form in the individual layers as a result of the rheological contrast between the layer and the adjacent layers (pinch-and-swell structures and boudins separated by planes of brittle failure, either extensional or shear fractures) and those that form as a result of the bulk mechanical anisotropy of the multilayer, which is determined by the intrinsic properties of the individual layers and the properties of the layer boundaries (normal kink bands and internal pinch-and-swell structures whose wavelength may be related to the thickness of an individual layer or group of layers).

The theory of deformation of mechanically anisotropic materials (Biot 1965) shows that the type of structure that develops when the principal compression is normal to the fabric or layering (normal kink bands or internal pinch-and-swell structures) depends on the magnitude of the anisotropy. However, the theory is a first increment theory and therefore cannot be used to investigate the amplification of pinch-and-swell structures and kink bands into finite structures.

The experimental work presented in this paper is used to show how these two types of structure amplify. The experiments show how single-layer features such as boudin necks can provide the necessary perturbations in the adjacent anisotropic matrix to initiate internal pinch-and-swell structures or normal kink bands and how these two structures, theoretically constrained to form in different materials, can develop together.

In the first part of the paper, a brief review is given of some of the experimental and theoretical work carried out in an attempt to understand the formation of boudins and related structures (for a more detailed discussion, see Price & Cosgrove 1990, pp. 405–431). This is followed by a discussion of the experimental work carried out by the present authors.

## PREVIOUS WORK

Over the past 15 years, numerous papers on boudinage and related structures have been published. This work has involved theoretical analyses (Lloyd & Ferguson 1982, Neurath & Smith 1982, Ghosh 1988, Mandal *et al.* 1992), field observations (Goldstein 1988, Lacassin 1988, Lacassin *et al.* 1993), and experimental investigation (Lloyd & Ferguson 1981, Neurath & Smith 1982, Hanmer 1986, Ghosh 1988, Goldstein 1988, Jordan 1991).

Most of the analytical and experimental work on layer normal compression deformation has been concerned with single layers. Ramberg (1955) was the first to present an analysis of the breakup of a single layer by extensional failure when subjected to layer normal compression. He considered a single competent, elastic layer sandwiched between two relatively weak viscous layers and derived an expression relating the tensile stress generated in the centre of a competent layer to the thickness of the layer ($H_1$) and matrix ($H_2$) and to the rate of compression normal to the layer, $\dot{e}_z$. It was assumed that the layer would deform by extensional failure and that after the initial tensile failure it would continue to divide into smaller sections (boudins) by successive 'mid-point' fracturing, until the boudins were too short to allow the layer parallel tensile stress within them to attain the tensile strength of the layer ($S$). The width, $W$, of the boudins formed in this manner is given by:

$$W = H_1 S \times \frac{H_2}{1.5\eta \,.\, \dot{e}_z}, \qquad (1)$$

where $\eta$ is the viscosity of the matrix.

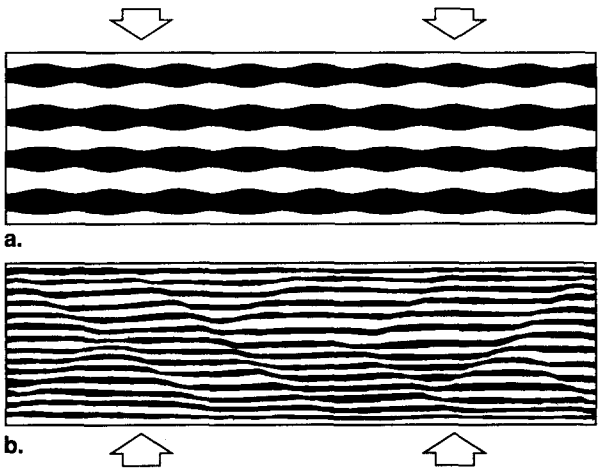


Fig. 1. Two types of structures: (a) interlocking pinch-and-swell structures; (b) conjugate normal kink bands, that can form when a homogeneous anisotropic material is compressed as shown by the arrows. The black and white bands represent passive markers which were originally parallel. Such structures also form in statistically homogeneous anisotropic materials such as mineral fabrics and multilayers. [(b) after Price & Cosgrove 1990.]

This equation indicates that the boudin width is governed by the thickness and tensile strength of the competent layer. Later work by Lloyd & Ferguson (1982) has confirmed Ramberg's model of mid-point fracture for the formation of rectangular boudins.

It is clear from field observations that competent layers do not always respond as brittle materials when compressed at a high angle to the layering. Instead, they may deform in a ductile manner and develop periodic thickening and thinning along their length. This leads to the formation of pinch-and-swell structures. Theoretical work presented by Smith (1975, 1977, 1979) shows that if there is a large competence contrast between the layer and the matrix and if the matrix and layer are not markedly non-linear, then the wavelength of these structures is given by:

$$\lambda = 2\pi H_1 \times \sqrt[3]{\frac{\eta_1}{6\eta_2}}, \qquad (2)$$

where $\eta_1$ and $\eta_2$ are measures of the resistance to deformation of the layer and matrix respectively.

Smith (1977) showed that if the layer and matrix are significantly non-linear, then the wavelength of the pinch-and-swell structure is given by:

$$\lambda = 2\pi H_1 \times \sqrt[3]{\frac{\eta_1}{6\eta_2}} \cdot \frac{n_2^{1/6}}{n_1^{1/3}}, \qquad (3)$$

where $n_1$ and $n_2$ are measures of the non-linearity of the layer and matrix respectively. If the materials are power-law materials, then $n$ is the exponent. It can be seen that for linear materials ($n = 1$) equation (3) reduces to equation (2).

Equation (2) is identical to the equation derived by Ramberg (1960) and Biot (1961) for the wavelength of the folds that form when a single layer with linear material properties set in a less competent linear matrix is compressed *parallel* to the layer.

The only theoretical analysis known to the authors that addresses the problem of boudin formation in multilayers is that of Strömgård (1973), who considered the formation and orientation of extension fractures in a regular bilaminate compressed normal, or at a high angle, to the layering. This work showed that the layers can be broken into rhomboidal boudins, provided that the maximum principal compression does not act exactly normal to the layers. Theoretical work on the formation of boudins and related structures in homogeneous, anisotropic materials such as slates and schists has been presented by Cobbold *et al.* (1971) and Sowers (1973). These workers used Biot's (1965) analysis of the deformation of mechanically anisotropic materials and showed that there are two types of structures that can develop when such a material is compressed at right-angles to the layering or fabric. These are interlocking pinch-and-swell structures and normal kink bands, shown in Fig. 1, and referred to as Type I and Type II structures respectively. Which structure forms is determined by the degree of anisotropy. Pinch-and-swell structures form in materials with a relatively low degree of anisotropy and normal kink bands in material where the anisotropy is well developed.

The theoretical work mentioned above has been successful in explaining how a brittle, competent layer breaks into rectangular boudins of a particular length by the process of mid-point fracture. It can also account for the formation of pinch-and-swell structures in a ductile competent layer and kink bands or pinch-and-swell structures in a mechanically anisotropic material. However, in order to understand how the structures predicted by these first increment theories grow into finite structures, it is necessary to use the techniques of numerical or analogue modelling.

One of the first attempts at numerical modelling of layer normal compression deformation was by Stephansson & Berner (1971), who used the technique of finite element analysis to determine the stress distribution in and around rectangular boudins as they

Fig. 2. Two stages in the layer normal compression of Model 1 (see Table 1) showing the development of tensile failure in the dark, more competent layers. (a) After 15.9% shortening; (b) after 12.5% shortening; (c) detail of (a).

Fig. 3. Plan view of a black 1 mm thick competent wax layer originally sandwiched between light-coloured, relatively incompetent layers, after 36% layer normal compression.

Fig. 4. Three stages in the deformation of Model 4 showing the formation of rhomboidal-shaped boudins in a single, relatively competent Plasticine layer compressed normal to the layering. See text for discussion.

Fig. 5. Three stages in the deformation of Model 5 showing the shear failure of two relatively competent Plasticine layers set in a less competent Plasticine matrix. See text for discussion.

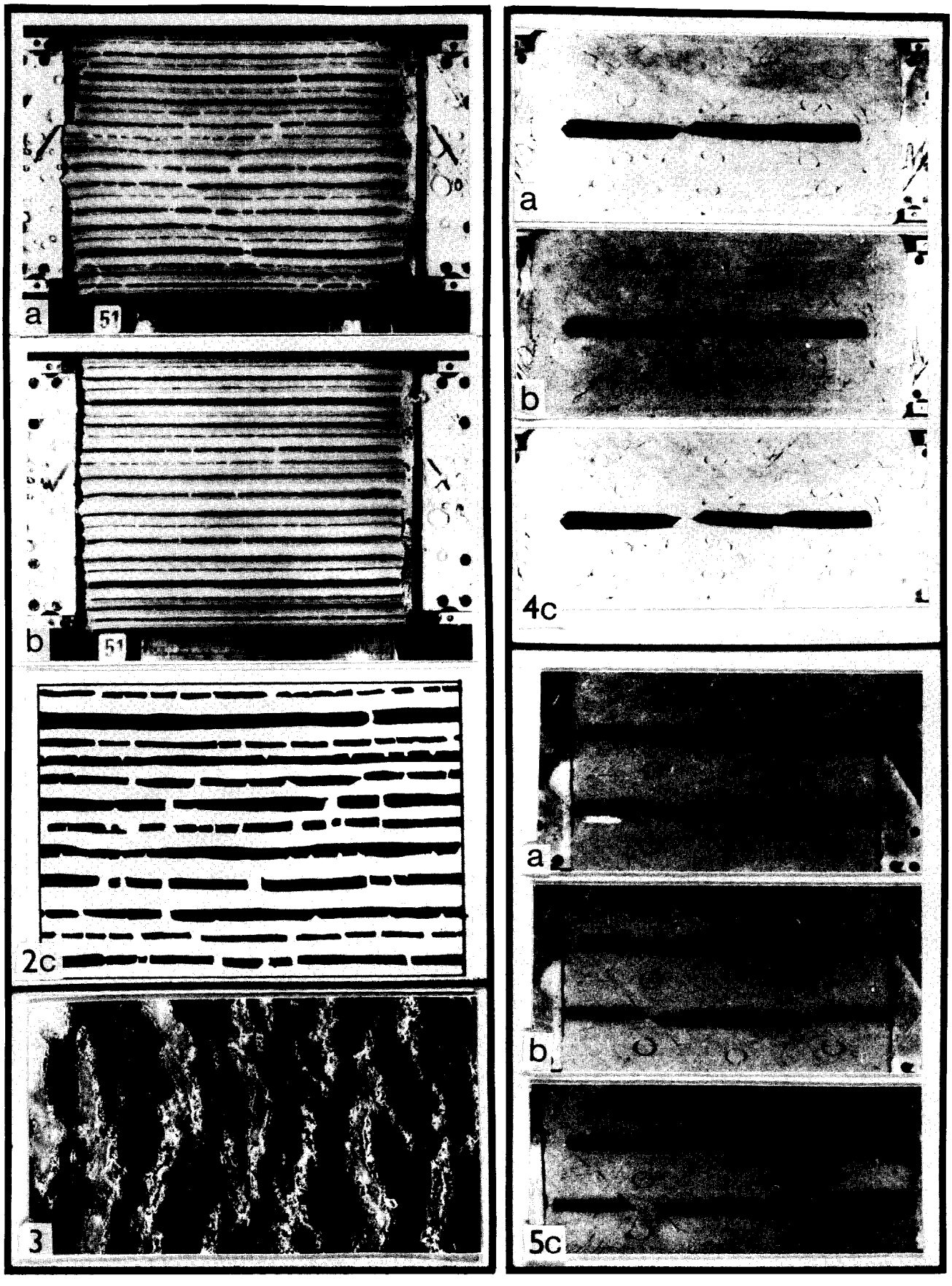


Figs. 2–5.


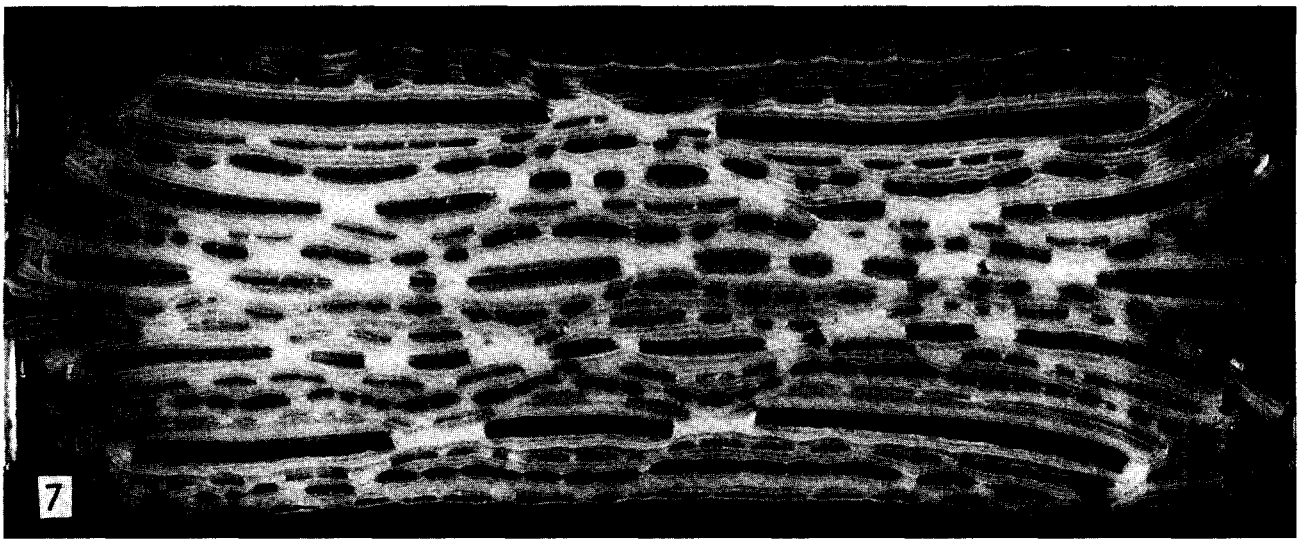


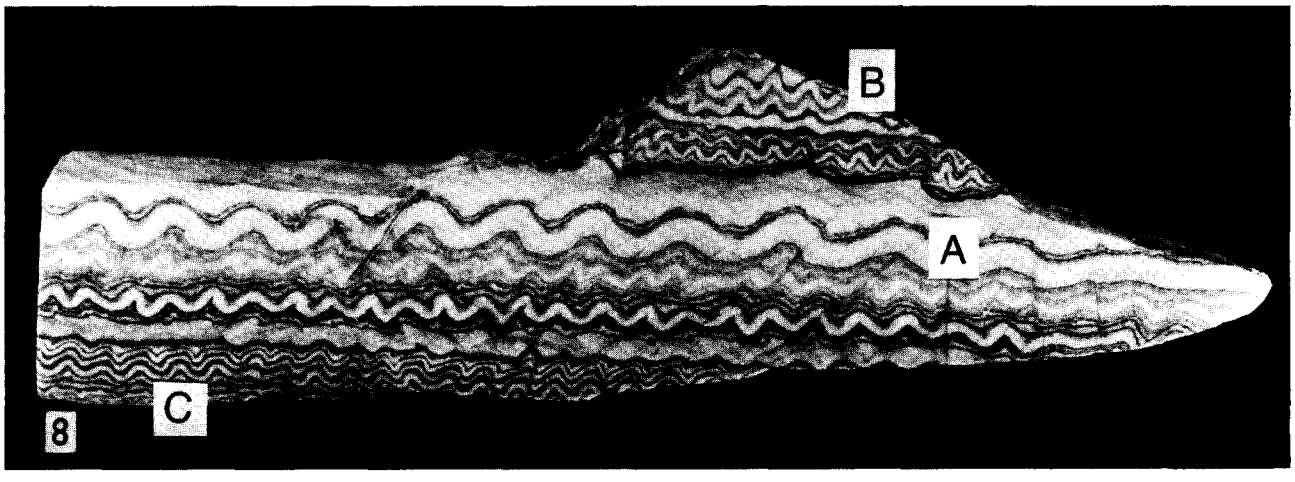


Fig. 6. Both (a) and (b) are schematic representations of Model 6 after 0% and 27% shortening respectively, showing the central relatively uniformly deformed region flanked by two horizons (stippled) in which pinch-and-swell structures and normal kink bands are forming. A close-up of these structures is shown in (c).

Fig. 7. Model 1 (see Fig. 2) after 36% shortening. The spatial relationship between the rectangular boudins, the pinch-and-swell structures and normal kink bands can be seen clearly.

Fig. 8. Folded multilayer from the Castile and Todillo evaporites of New Mexico, showing regions characterized by single-layer folding (A), multilayer folding (B) and the buckling of anisotropic materials (C). The different types of folding occur in different areas of the multilayer and appear to have developed independently of each other.

Table 1. Description of Models 1–6 referred to in the text and deformed in Experiments 1–6

| Model No. | Description | Temp. (°C) | Strain rate ($s^{-1}$) | Bulk shortening (%) | Structures |
|---|---|---|---|---|---|
| 1 | Multilayer of two 3 mm, three 2 mm and 19 1 mm thick black competent layers of 54°C m.pt. p.w* in a layered matrix of 1 mm thick white 50°C m.pt p.w. | 28.3 | $2.05 \times 10^{-4}$ | 36 | Tensile fractures, rectangular boudins |
| 2 | Same as above, but with the incompetent layers coloured orange | 28.3 | $2.05 \times 10^{-4}$ | 36 | Tensile fractures, rectangular boudins |
| 3 | Multilayer of 1 mm thick layers of 54°C m.pt. p.w. lubricated with silicon grease. A 1 mm thick layer of more competent 58°C m.pt. p.w. coloured black is placed every five yellow layers | 36 | $2.05 \times 10^{-4}$ | 37 | Lensoid boudins separated by tensile fractures |
| 4 | A single layer of black Plasticine, 0.5 cm thick, set in a matrix of soft pink Plasticine | 24.5 | $2.05 \times 10^{-4}$ | 37.3 | Rhomboidal boudins separated by shear fractures |
| 5 | Two layers of black Plasticine, 0.5 cm thick, set in a matrix of soft pink Plasticine | 24.5 | $2.05 \times 10^{-4}$ | 27.6 | Rhomboidal boudins separated by shear fractures |
| 6 | Multilayer consisting of alternating light and dark layers of 54°C m.pt. p.w., each 1 mm thick, lubricated with silicon grease | 36 | $2.05 \times 10^{-4}$ | 40 | Internal pinch-and-swell structures and normal kink bands |

*m.pt. p.w. = melting point paraffin wax.

Table 2. Variation in the per cent shortening across Model 6, shown in Fig. 6. The table gives the per cent strain in the upper and lower strain softened zones and in the central zone in which no strain softening has occurred, for three values of per cent bulk shortening

| Bulk shortening (%) | 27 | 31.5 | 40 |
|---|---|---|---|
| Upper strain-softened zone | 33 | 36.7 | 45.5 |
| Central zone of no strain-softening | 18.1 | 20.2 | 25 |
| Lower strain softened zone | 31 | 34 | 42.75 |

deformed and separated during layer normal compression. They showed that the stress distribution is compatible with the redistribution of minerals found to occur around natural boudins and that there was a tendency for the boudins to become barrel-shaped as the deformation increased and the boudins separated. Later, Lloyd & Ferguson (1981, 1982) successfully investigated the process of 'mid-point' fracture using elastic–plastic finite element simulations.

Like the analytical studies, most analogue modelling of layer normal compression deformation has been focused on single-layer structures deformed either in pure shear (Neurath & Smith 1982, Ghosh 1988, Mandal *et al.* 1992) or simple shear, these latter experimental studies investigating the possible use of these structures as kinematic indicators. For example, Hanmer (1986) studied the effect of simple shear deformation on originally symmetric boudins separated from each other by extensional fractures normal to the layer boundary, while Jordan (1991) and Goldstein (1988) considered the effect of such a deformation on rhomboidal boudins separated from each other by shear fractures. A review of the use of boudins and pinch-and-swell structures as kinematic indicators is given by Hanmer & Passchier (1991).

Surprisingly little analogue modelling has been carried out to investigate the formation of boudins and related structures in multilayers (Woldekidan 1982). The experimental work described in this article considers the initiation and finite development of a variety of structures in a complex multilayer (i.e. one made up of a variety of different layers with different thicknesses and competencies) when it is deformed in pure shear by the maximum principal compressive stress acting normal to the layering. The experiments show how the individual structures such as boudins and single-layer pinch-and-swell structures (which relate to the relative rheologies of adjacent layers) and normal kink bands and large scale pinch-and-swell structures (which relate to the bulk mechanical anisotropy of the multilayers) interact, as well as how the formation and amplification of one type of structure initiates another.

## THE EXPERIMENTS

### *Apparatus, model materials and experimental procedure*

The apparatus used for the experiments was a pure shear deformation rig, a detailed description of which is given in Cobbold (1975). The output shaft of the gear box is an eccentric cam, which varies the angular velocity with time so as to deform the model at a constant strain rate. Four rotary shafts to which rotors are connected turn synchronously, driving the two pistons together. The load is transmitted from the rotors to the pistons via journal bearings and is measured with resistance strain gauges fixed to the axes of each shaft. The models, which were made up of layers 15 cm long, 5 cm wide and of various thicknesses ranging from 1 to 10 mm, had initial dimensions of $X = 15$ cm, $Z = 15$ cm and $Y = 5$ cm and

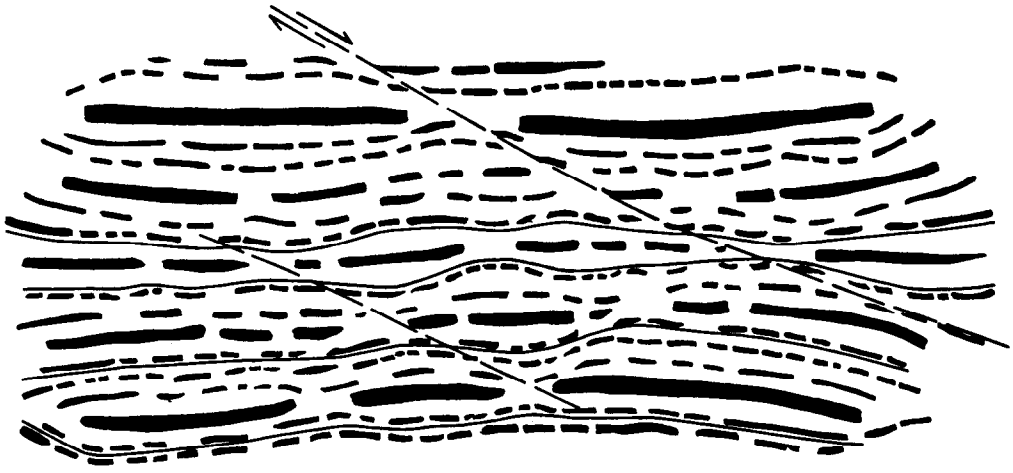

Fig. 9. Line drawing of Fig. 7, showing the spatial relationship between the rectangular boudins in the thick competent layers (dark), the large scale pinch-and-swell instabilities indicated by the solid lines and the conjugate normal kink bands indicated by the dashed lines.

were deformed under controlled conditions of strain rate and temperature. Throughout the experiments, $X$ and $Z$ varied but $Y$ was constrained to remain constant. A few experiments were performed on Plasticine models, but the majority consisted of paraffin wax layers of various melting points (50°C, 54°C and 58°C). Paraffin wax was chosen because its rheological properties vary between brittle and ductile over the temperature range that can be used conveniently in the apparatus.

A simple method was used for preparing wax in the form of thin sheets (see Summers 1979). This method makes use of the low specific gravity of wax and involves the floating and cooling of a thin sheet of molten wax on the surface of a water bath. The wax layers were then cut and stacked to form the multilayers and the layers separated from each other by a thin film of silicon grease.

Although over 50 experiments were performed to investigate the effect of layer normal compression on the deformation behaviour of a multilayer, the resulting structures can be illustrated by reference to the six listed in Table 1. The models deformed during these experiments together with the structures that formed will now be discussed. The structures can be sub-divided into those related to single-layer behaviour and those that form as a result of the mechanical anisotropy of the multilayer.

When single competent layers within a multilayer being compressed normal to the layering behave as brittle materials, they may fail by either tensile or shear failure. In the experiments described in this paper, it was noted that the competent layers in the wax multilayers tended to fail by tensile failure and those in putty multilayers failed by shear. Experiments exhibiting these two modes of deformation will be considered in turn.

*Boudins generated by the tensile failure of individual competent layers*

It was observed that, when the competent layers failed by tensile failure normal to the layering, the adjacent incompetent material flowed into the gap which developed between the separating rectangular boudins. In the low temperature experiments (28°C), the boudins remained rectangular as deformation proceeded. In the relatively high temperature experiments (36°C), they became lenticular as the matrix flowed into the gaps.

Experiment 1 (Table 1, Fig. 2) illustrates the formation of rectangular boudins and the development of a well-defined width thickness ratio by a process of midpoint failure of relatively large boudins.

After 8% bulk strain (21 min), tension fractures had appeared in four of the 1 mm thick competent layers, although some of the fractures had not cut completely through the layers. After 10% strain, fractures appeared in other 1 mm thick layers and tensile failure had been initiated in two of the 2 mm thick layers. After 12.5% strain, only the 3 mm thick layers remained unfractured (Fig. 2a). The average width of the boudins (i.e. the distance between the two adjacent fractures) decreased with deformation and at any stage in the deformation the number of tension fractures in any layer was found to be inversely proportional to its thickness. Tensile failure occurred in the lower 3 mm competent layer after 13% shortening and Fig. 2(a) shows the model after 15.9% shortening. Structures that formed during the continued deformation of this model are described in the discussion and illustrated in Figs. 7 and 9.

*The effect of thickness on fracture spacing*

Models 1 and 2 (Table 1) both contain 24 relatively competent layers of paraffin wax (two 3 mm thick layers, three 2 mm thick layers and 19 1 mm thick layers) and a schematic representation of six 1 mm thick competent layers (three each from experiments 1 and 2) at various stages of deformation is shown in Fig. 10. After 36% bulk shortening, the average number of boudins for the three layers of Model 1 is 36 and for those of Model 2 is 37.

In the early stages of an experiment, relatively few tension fractures develop in the initially continuous competent layers. These often divide the layer into

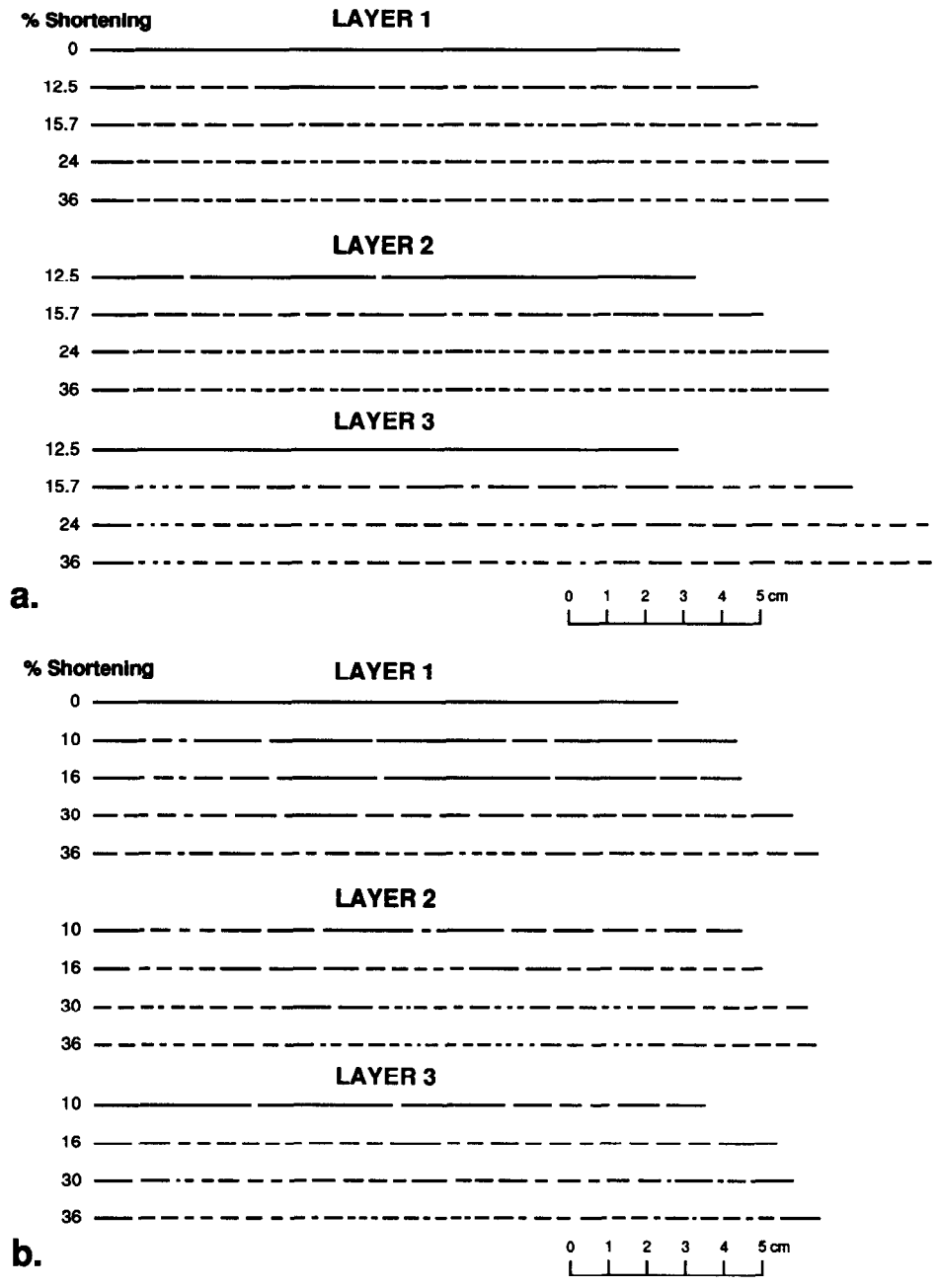


Fig. 10. Schematic representation of six 1 mm thick competent layers; (a) three from Experiment 1; (b) three from Experiment 2, at various stages in the compression of the models.

boudins of considerably different widths. During continued deformation, the boudins are then broken down into smaller boudins by the development of new tension fractures. The position of these new fractures has been studied and the ratio of the widths of the boudins formed from a larger boudin recorded during the deformation of Models 1 and 2. The results are shown as histograms in Fig. 11.

It can be seen from these histograms (particularly c & d) that statistically each boudin breaks into two boudins of equal width as the theory of fibre loading (Ramberg 1955) and fracture spacing predict. However, the spread of the histograms indicates that this does not always happen and that splitting in the ratios of up to 1:4 may occur as can be seen from the experimental results shown in Fig. 10. It might be argued that the splitting into ratios other than 1:1 is a consequence of the boundary conditions of the experiments. However, many geological examples show boudins divided into a similar range of ratios (see e.g. Lloyd & Ferguson 1982).

The histograms of boudin width in Experiments 1 and 2 after 36% shortening are shown in Figs. 12(a) & (b) respectively. A dominant fracture spacing (boudin width) is apparent, although a broad spread of boudin widths developed.

It can be seen from the histograms of Fig. 13, which show the boudin widths in the 1 mm competent layers of Model 2 at various stages of its deformation, that the dominant width of boudin, associated with a particular layer thickness, becomes apparent even after a relatively

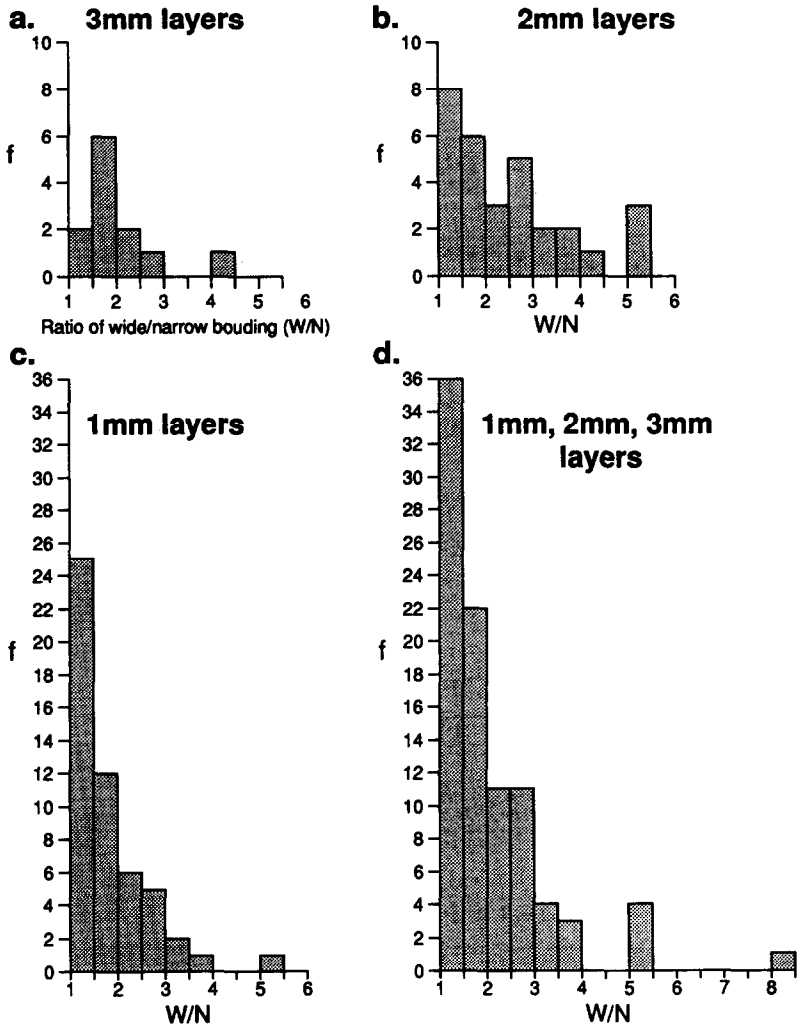


Fig. 11. Histograms showing the width ratios of wide to narrow boudins that result from tensile failure of a larger boudin in the (a) 3 mm, (b) 2 mm, (c) 1 mm thick competent layers of Experiments 1 and 2; (d) shows the combined results from (a), (b) and (c).

small amount of deformation. The optimum boudin width (4 mm) that developed in the 1 mm thick competent layers can be seen clearly from the histogram after only 16% shortening. In natural examples of boudins, a fairly constant boudin width is generally observed to occur in a particular layer. However, as pointed out above, boudin widths in some competent horizons are sometimes seen to vary considerably (Lloyd & Ferguson 1982). These workers, who developed a stress transfer theory for the initiation of boudins, measured 91 quartzite boudins within the Lower Carboniferous slates of Tintagel, Cornwall and found that the predicted aspect ratios (width/thickness) were in close agreement with those measured in the field. They concluded that natural rock layers are likely to contain randomly distributed inbuilt flaws and assumed that the number of such flaws per unit length of layer can be estimated by recognizing that, in any stress transfer mechanism, the largest gaps correspond to the earliest fracture sites. This can be clearly seen from Fig.7.

The graph of Fig. 14(a) shows the plot of percentage strain against the average width of the boudin for competent layers 1 mm, 2 mm and 3 mm thick in Experiment 1 (Table 1). The graphs show that the width of the boudins decreases as the strain increases until a particular width is attained. Beyond this stage in the deformation, no further fracturing (i.e. no further reduction in boudin width) occurs.

The plots of the average width/thickness ($W/H$) ratio of boudins against the percentage shortening for the 1 mm, 2 mm and 3 mm thick competent layers of Models 1 and 2 are shown in Fig 14(b). It can be seen from these graphs that the fracture spacing in a particular layer varies in a non-linear way during the progressive deformation. The graph of Fig. 14(c) shows the plot of layer thickness against the average width of the boudins at different stages in the shortening of the models. The curves indicate that, statistically, the relationship between the thickness and width of the boudins at a particular stage of the deformation is approximately linear.

One of the advantages of paraffin wax as a model material is that the multilayers can be dismantled after the experiments have been performed and the boudin geometry in the plane of the layering can be studied. Such a 'plan' view of a 1 mm thick competent layer from

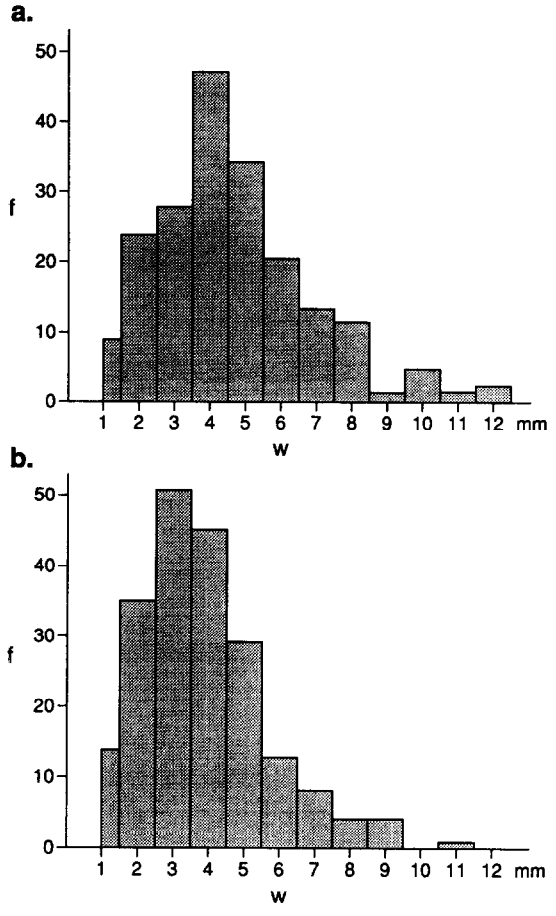


Fig. 12. Histograms of boudin width in the 1 mm thick competent layers after 36% shortening (a) in Experiment 1; (b) in Experiment 2.

Experiment 1 is shown in Fig. 3. It can be seen that the boudins are remarkably non-cylindrical (see Ghosh 1988).

*The effect of temperature on boudin geometry*

One of the properties of paraffin wax which makes it such a useful model material is that its rheology is very sensitive to temperature. At the strain rates used in the experiments ($2.05 \times 10^{-4}\ s^{-1}$), the behaviour changes from brittle to ductile over a temperature range of less than 20°C. In experiments conducted at relatively low temperatures (28°C for Model 1, Table 1), rectangular boudins formed in the higher melting point (54°C) wax layers, which behaved in a brittle manner (Fig. 2). In the high temperature experiments (36°C for Model 3, Table 1), lenticular boudins formed in the 54°C m.pt. wax layers which necked before separating. In this model, the average width of the boudins in the 1 mm thick competent layers is more than in Model 1, a relatively low temperature experiment. The reason for this is that extension of the competent layer in the higher temperature experiment is achieved by a combination of ductile flow and brittle fracture, whereas in the low temperature experiment the extension is achieved predominantly by brittle failure.

*Boudins generated by shear failure in individual competent layers*

As noted earlier, shear failure of individual competent layers only occurred in the models made of Plasticine. Two experiments will be described, one on a model containing a single layer of relatively competent standard black Plasticine set in a matrix of special soft unlayered Plasticine, and the other on a model containing two competent layers in a soft, unlayered Plasticine matrix. Both experiments were carried out at room temperature and there was no lubricant between the layers and the matrix.

In the first experiment (Model 4, Table 1, Fig. 4), shear planes initially appeared in the matrix after 25 min at a strain rate of $2.05 \times 10^{-4}\ s^{-1}$. Later, after 23% bulk shortening, a shear plane developed in the competent layer at 40° to $\sigma_1$; Fig. 4(b). After 26% shortening, whilst layer separation was occurring at the first fracture, a second shear was initiated in the longer segment of the layer also at 40° to the compression direction. Neither fault in the competent layer was the continuation of a fault in the matrix. After 29% shortening, the segments on either side of the first fault in the layer had completely separated and the segment between the two faults became more apparent (Fig. 4c). It had a thickness:width ratio of 1:5. At the end of the experiment (33% bulk strain), the first and second shear planes in the layer had rotated to 47° and 46° to the compression direction respectively.

The second experiment (Model 5, Table 1), in which the boudins formed by shear failure, contained two competent layers (Fig. 5). As in the single-layer experiment described above, shear failure first appeared in the matrix. After 14% bulk shortening, shear failure (Fault 1) occurred in the lower layer at 44° to the compression direction (Fig. 5a). After 19% shortening, this angle had increased to 47° and two other shear planes (Faults 2, top layer, and 3), conjugate to the first and both inclined at 42° to the compression direction, appeared (Fig. 5b). Fault 2 was initiated in the layer and subsequently extended into the matrix, whereas Fault 3 formed in the matrix and extended into the layer. As deformation continued, new shear planes (e.g. Fault 4) were initiated and movements on and rotation of Faults 1 and 3 modified the geometry of layers, giving them the appearance of pinch-and-swell structures that had been separated and slightly displaced. The amount of rotation of the faults increased as deformation continued and, by the end of the experiment (29% shortening), Fault 1 had rotated to 50° to $\sigma_1$.

*Structures resulting from multilayer behaviour*

The structures formed in Experiments 1–5 and illustrated in Figs. 2, 4 and 5 are the result of brittle failure of single competent layers by either tensile or shear failure. However, when a complex multilayer is compressed normal to the layering, its response it often governed by its bulk mechanical anisotropy rather than by the properties of an individual competent layer. When this

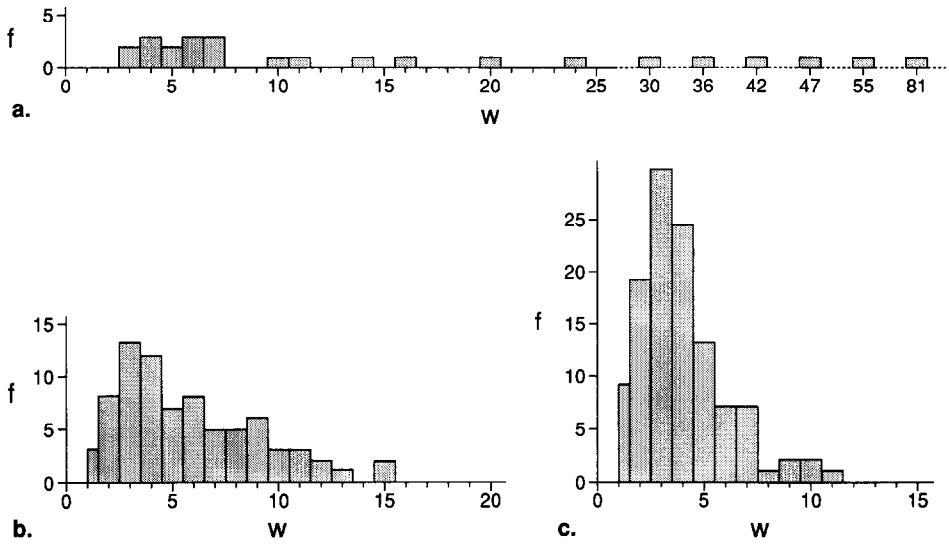


Fig. 13. Histograms showing the width of boudins in the 1 mm thick competent layers of Model 2 after (a) 10%; (b) 16% (c) 30% shortening.

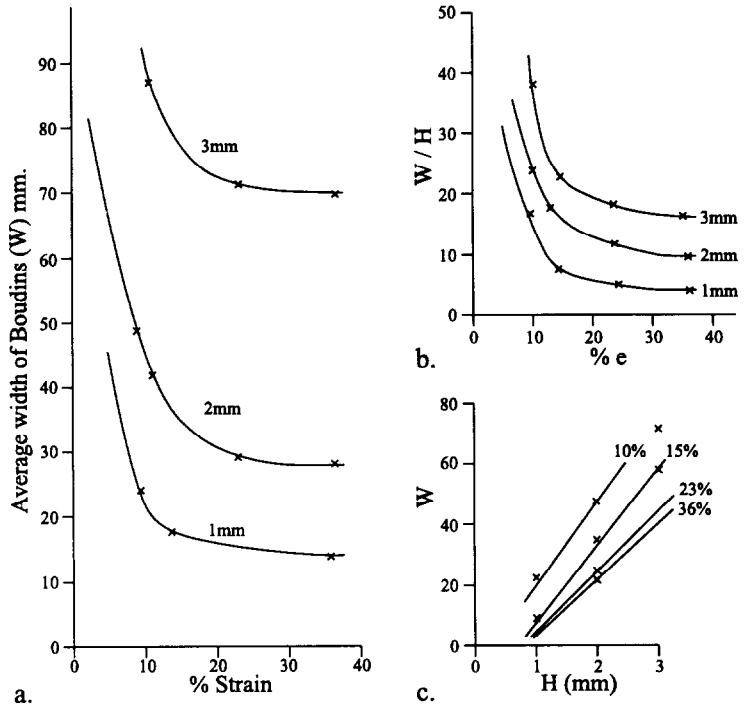


Fig. 14. (a) Plot of percentage strain against the average boudin width for the 1 mm, 2 mm and 3 mm thick competent layers in Experiment 1; (b) the average width/thickness ratio ($W/H$) of the boudins plotted against percentage shortening for the 1 mm, 2 mm and 3 mm thick competent layers of Experiments 1 and 2; (c) plot of layer thickness against average boudin width at different stages in the shortening of Models 1 and 2.

occurs, it has been demonstrated theoretically (Cobbold *et al.* 1971) that either interlocking pinch-and-swell structures or a network of conjugate normal kink bands may form (Fig. 1).

The formation of these structures is well illustrated in Model 6 (Table 1), which is made up of alternating dark and light layers of 54°C melting point wax, each approximately 1 mm thick (Fig. 6). The layers are separated from each other by a thin film of silicon grease (approximately $1.6 \times 10^{-3}$ mm thick) which allows almost frictionless slip to occur between the layers. Thus, although there is no competence contrast between the individual layers making up the multilayer, it is highly anisotropic. Compression was applied normal to the layering and after 10% bulk shortening, pinch-and-swell structures started to form near the pistons (top and bottom of Figs. 6a & b).

As the layers close to the piston face developed pinch-and-swell structures, they affected the adjacent, relatively undeformed layers, the swells favouring the formation of necks in the adjacent layers and the necks the formation of swells. In this way the zone of deformation spread from both piston faces towards the centre of the model. This migration continued until the zone contain-

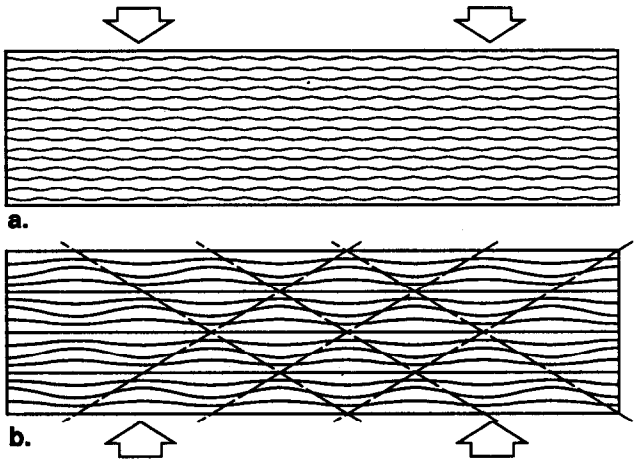


Fig. 15. Internal pinch-and-swell structures developed (a) on the scale of the individual layers making up the multilayer; (b) on a larger scale involving four layers. Note that the geometry of these structures is equivalent to a network of conjugate normal kink bands parallel to the dashed lines.

ing pinch-and-swell structures was approximately 2.5 cm wide (20% of the width of the model). The zones then effectively ceased to widen and subsequent deformation was concentrated within them. The result is a central zone which is relatively undeformed sandwiched between two more deformed zones (stippled in Fig. 6b) in which pinch-and-swell structures are developed.

Initially, the individual pinch-and-swell structures are amplified at the same rate; however, after 12% bulk shortening of Model 6, it was observed that this relatively uniform deformation gave way to a more localized one in which deformation was concentrated along a diagonal array of pinched regions (necks) which linked in such a way as to form well-defined normal kink bands parallel to the conjugate directions indicated by the dashed lines on Fig. 15(b). The bands were initially inclined at approximately 30° to the layering, but this angle was reduced as deformation continued. After the bulk shortening had reached 27%, the angle had been reduced from 30° to 25° and by the end of the experiment (40% bulk shortening) this angle had been reduced to 22°.

The localization of instabilities in zones close to the pistons occurred in several experiments. In some, the individual layers developed pinch-and-swell structures; in others, the structures developed on a larger scale and the units undergoing regular thickening and thinning were made up of several layers (see Figs. 6 and 15).

It can be seen from Fig. 15 that the deflection of the layer boundaries that accompanies the formation of interlocking pinch-and-swell structures is such that a network of overlapping conjugate normal kink bands is defined (the two sets of dashed lines). We return to this point in the discussion when the relationship between the two structures is considered further.

The experiments were carried out at a constant strain rate and the variation in stress during the deformation indicated important rheological changes occurring within the models. A plot of the (bulk) shortening against the average stress during the deformation of

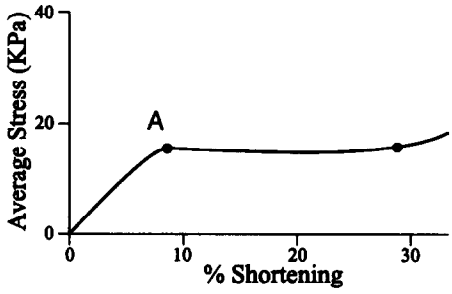


Fig. 16. Plot of the average (bulk) shortening against the average stress during the deformation of Model 6. 'A' represents the onset of strain softening and coincides with the initiation of pinch-and-swell structures in the layers adjacent to the pistons. See text.

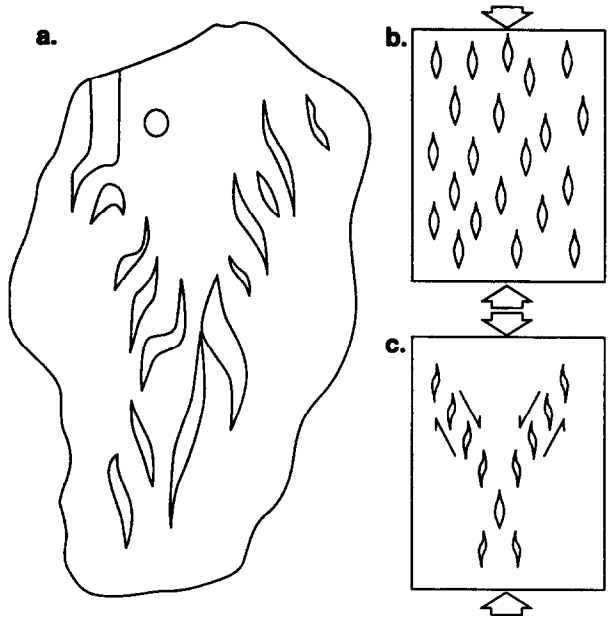


Fig. 17. (a) Field sketch of a conjugate set of en échelon tension gashes. (b) A uniform distribution of tension gashes representing tensile failure. (c) The organization of tension gashes to produce localized shear failure.

Model 6 is shown in Fig. 16. The stress is seen to increase until the appearance of the first pinch-and-swell structures (point A, Fig. 16) when it drops slightly. The deformation then continues at an almost constant stress until approximately 30% bulk shortening has occurred. This break in slope of the stress–strain curve denotes the onset of strain softening which is associated with the formation of pinch-and-swell structures and the associated local changes in orientation of the layering.

The formation of pinch-and-swell structures in zones adjacent to the pistons divides the model into a central competent 'layer' sandwiched between two relatively weak layers in which strain softening has occurred. Thus, as deformation continues, greater shortening will occur across the weak layers than across the stronger layer. The variation of layer normal shortening across the model at various stages of deformation is given in Table 2. It might be expected, therefore, that the competent central 'layer' would develop boudinage structures in the same way as a single competent layer does when compressed between two incompetent horizons.

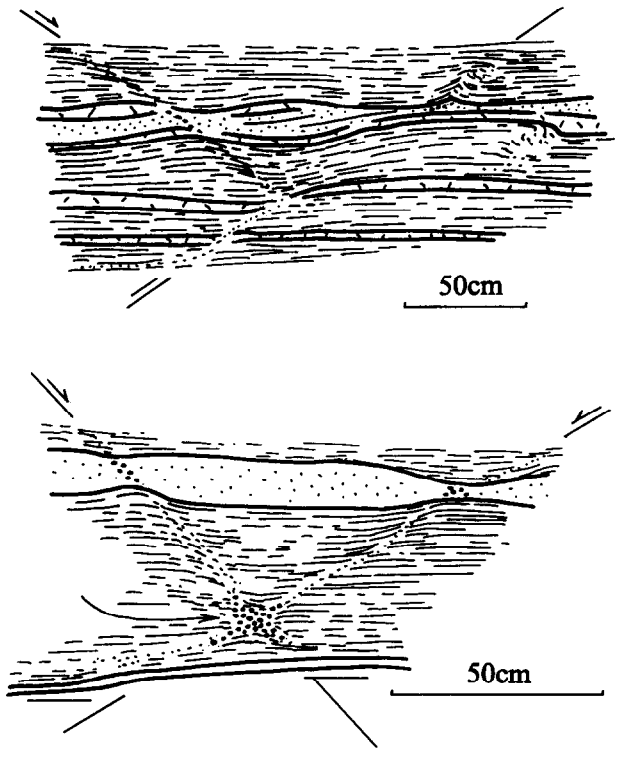


Fig. 18. Natural examples of the deflection of an anisotropic matrix into a neck region of a pinch-and-swell structure initiating normal kink bands (after Halbich 1978).

The central layer in Fig. 6(b) can be envisaged as representing a single boudin.

## DISCUSSION

The structures resulting from layer normal compression of a variety of model multilayers can be accounted for in terms of either the theory of single-layer deformation or in terms of the deformation behaviour of statistically homogeneous, mechanically anisotropic materials.

In the experiments, the single competent layers failed either by tensile or shear failure and the structures associated with tensile failure have geometries which range from well-separated rectangular boudins to slightly detached, lozenge-shaped boudins, depending upon the rheology of the layer and the amount of deformation. Brittle behaviour and large deformations favour the former and more ductile behaviour the latter.

Shear failure of a single competent layer forms boudins that are rhomboidal. Their geometry can become considerably modified by subsequent deformation so that they become difficult to distinguish from pinch-and-swell structures, particularly if the shear failure is accompanied by an element of ductile deformation.

When the deformation of a multilayer is governed by its bulk mechanical anisotropy, two distinct types of structures may result. These are internal pinch-and-swell structures and normal kink bands and, as mentioned earlier, these two structures correspond to two types of instability referred to as Type I and Type II. The degree of anisotropy of the material controls which structure will form. Thus, the theory predicts that either one or other of the structures (but not both) will develop depending on the anisotropy of the deforming material. However, the theory cannot be used to predict how these structures amplify and it is during their growth into finite structures, which can be examined during the deformation of the models, that the difference between them, so apparent from the theory, becomes less clear. For example, in the experiments involving multilayers made up of identical layers separated by a thin film of lubricant, it was found that these two structures almost invariably occur together. In more complex multilayers, i.e. multilayers made up of a variety of different layers with different thicknesses and different properties, deformational behaviour characteristic of both single layers and anisotropic materials often occurred together. These experiments give an interesting insight into the spatial and temporal relationships that sometimes exist between the various types of layer normal compression instabilities. This is clearly illustrated in Model 1, shown in Figs. 2, 7 and 9. The first structures to form were rectangular boudins (Figs. 2a & c). With progressive deformation, deflection of the layered matrix into the neck region between separating rectangular boudins generated a series of interlocking pinch-and-swell structures (Fig. 7). With continued deformation, the pinch-and-swell structures amplified and normal kink bands, which formed by the linking of various neck regions in the pinch-and-swell array, became apparent (Figs. 7 and 9). A similar relationship between the formation of pinch-and-swell structures and conjugate normal kink bands occurred in Model 6 (Fig. 6), where it was noted that the individual pinch-and-swell structures initially amplified at the same rate. Later, this relatively uniform deformation gave way to a more localized one in which deformation was concentrated along a diagonal array of pinched regions (necks) which linked in such a way as to form well-defined normal kink bands.

This relationship between internal pinch-and-swell structures and normal kink bands has a sound mathematical basis (Biot 1965) which becomes clear when the displacements associated with the two instabilities are considered. The displacement pattern associated with internal pinch-and-swell structures is equivalent to the *superposition* of two opposing simple shears parallel to the characteristic directions (dashed lines in Fig. 15b) whereas the formation of conjugate normal kink bands is equivalent to the *juxtaposition* of two apposing simple shears parallel to the characteristic directions (Fig. 1b). The pinch-and-swell structures represent a relatively pervasive deformation (Fig. 1a) and the normal kink bands a more localized deformation (Fig. 1b). However, it is clear from Fig. 15(b) that if conjugate normal kink bands are sufficiently closely spaced then the result will be a symmetric network of shears with a geometry indistinguishable from an array of interlocking pinch-and-swell structures.

The relationship between pinch-and-swell structures

and normal kink bands also highlights an interesting link between tensile and shear failure. The pinch-and-swell structures, which produce a symmetric and periodic necking of the layers, are an expression of tensile yielding or failure. However, it has been noted that as deformation continues these zones of yielding (the necks) link to form a planar zone of localized shear deformation (the normal kink band). This process finds a parallel in brittle deformation where (bulk) shear failure is often achieved by the linking of individual tension fractures in an en échelon array (Fig. 17).

In some experiments, an originally uniform anisotropic material became more complex during deformation by the development of horizons in which strain softening occurred as a result of the formation of pinch-and-swell structures and normal kink bands (Fig. 6). As can be seen from Fig. 6, the division of the originally uniform material into competent and relatively incompetent layers (the layers in which strain softening has occurred) may result in the formation of boudins in the relatively competent layers.

It is also clear from the experiments that the various layer normal compression structures may develop on a variety of scales when complex multilayers are deformed. Three scales of pinch-and-swell structures can be seen in the experiments. These are illustrated in Figs. 6, 7, 9 and 15. Figure 15(a) shows the structures forming on the scale of the individual layers making up the multilayer and Figs. 15(b) and 6 show them on a larger scale involving four and 11 layers respectively. Even larger pinch-and-swell structures (involving 16 layers), developed in Experiment 1, are shown in Figs. 7 and 9.

The analyses of Smith (1977, 1979) show that pinch-and-swell instabilities are in general much weaker than folding instabilities. For pinch-and-swell the dynamic and kinematic growth rates are of opposite sign, whereas for folding they are of the same sign. Thus, for given materials, folds in shortening are more likely to occur than pinch-and-swell in extension. It follows that the role of the perturbation from which a structure grows will be more important in the development of layer normal compression structures than in layer parallel compression structures and it is not surprising to find that in both the experiments described in this paper and in many natural examples (Fig. 18), layer normal compression structures can often be traced back to their source perturbation. For example, the normal kink bands in Figs. 7, 9 and 18 were initiated by the deflection of the layered matrix into the boudin neck regions that formed in the thick competent layers.

Some of the similarities and differences between the deformation behaviour of a complex multilayer subjected to layer normal and layer parallel compression can be seen by comparing the multilayers shown in Figs. 7 and 8. Both multilayers show structures characteristic of single-layer behaviour and the behaviour of a mechanically anisotropic material. However, whereas the two types of behaviour are intimately related both in time and space in the multilayer subjected to layer normal compression (see Figs. 7 and 9 and the accompanying discussion), in the multilayer deformed by layer parallel compression the various types of buckling behaviour, e.g. single layer buckling (Fig. 8A), multilayer buckling (Fig. 8B) and the buckling of anisotropic material (Fig. 8C) are found in separate horizons and there is no indication of one type of structure initiating another.

## CONCLUSIONS

Experimental work on multilayers compressed normal to the layering indicates that the structures that form may be controlled either by the properties of various single layers within the multilayer or by the mechanical anisotropy of the multilayer as a whole. A variety of structures was formed, including rectangular and rhomboidal boudins, pinch-and-swell structures and normal kink bands. It is argued that although structures formed during layer normal and layer parallel compression are the result of the same basic instability, layer normal compression structures are more difficult to initiate and their rate of growth is significantly lower than that of layer parallel compression structures. This may in part account for their intimate spatial and temporal relationship compared with the various types of layer parallel compression structures; i.e. the generation of one structure such as a boudin may provide the disturbance necessary for the initiation of another, often quite different, structure such as a normal kink band.

## REFERENCES


Biot, M. A. 1961. Theory of folding of stratified visco-elastic media and its implications in tectonics and orogenesis. *Geol. Soc. Am. Bull.* **72**, 1595–1620.

Biot, M. A. 1965. *Mechanics of Incremental Deformation*. Wiley, New York.

Cobbold, P. R. 1975. A biaxial press for model deformation and rheological tests. *Tectonophysics* **26**, T1–T5.

Cobbold, P. R., Cosgrove, J. W. & Summers, J. M. 1971. Development of internal structures in deformed anisotropic rocks. *Tectonophysics* **12**, 23–53.

Ghosh, S. K. 1988. Theory of chocolate tablet boudinage. *J. Struct. Geol.* **10**, 541–553.

Goldstein, A. G. 1988. Factors affecting the kinematic interpretation of asymmetric boudinage in shear zones. *J. Struct. Geol.* **10**, 707–716.

Halbich, I. W. 1978. Minor structures in gneiss and the origin of steep structures in the Okiep Copper District. *Geol. Soc. South Africa* Special Publication **4**(18).

Hanmer, S. 1986. Asymmetrical pull-aparts and foliation fish as kinematic indicators. *J. Struct. Geol.* **8**, 111–122.

Hanmer, S. & Passchier, C. 1991. Shear-sense indicators: a review. *Geol. Surv. Pap. Can.* **90**, 17.

Jordan, P. G. 1991. Development of asymmetric shale pull-aparts in evaporite shear zones. *J. Struct. Geol.* **13**, 399–409.

Lacassin, R. 1988. Large-scale foliation boudinage in gneisses. *J. Struct. Geol.* **10**, 643–647.

Lacassin, R., Lewup, P. H. & Tapponnier, P. 1993. Bounds on the strain on large Tertiary shear zones of SE Asia from boudinage restoration. *J. Struct. Geol.* **15**, 677–692.

Lloyd, G. E. & Ferguson, C. C. 1981. Boudinage structures: some interpretations based on elastic–plastic finite element simulations. *J. Struct. Geol.* **3**, 117–128.

Lloyd, G. E. & Ferguson, C. C. 1982. A stress transfer model for the development of extension fracture boudinage. *J. Struct. Geol.* **4**, 355–372.

Lohest, M. 1909. De l'origine des veines et de géodes des terrains primaries de Belgique. Troisieme note. *Annls Soc. géol. Belg.* **36**(*Bull.* 1908–1909), 275–282.

Mandal, N., Khan, D. & Deb, S. K. 1992. An experimental approach to wide-necked pinch-and-swell structures. *J. Struct. Geol.* **14**, 395–403.

Neurath, C. & Smith, R. B. 1982. The effect of material properties on growth rates of folding and boudinage: experiments with wax models. *J. Struct. Geol.* **4**, 214–219.

Price, N. J. & Cosgrove, J. W. 1990. *Analysis of Geological Structures*. Cambridge University Press, U.K.

Ramberg, H. 1955. Natural and experimental boudinage and pinch-and-swell structures. *J. Geol.* **63**, 512–526.

Ramberg, H. 1960. Relationships between lengths of arc and thickness of ptygmatically folded veins. *Am. J. Sci.* **258**, 36–46.

Smith, R. B. 1975. Unified theory of the onset of folding, boudinage and mullion structure. *Geol. Soc. Am. Bull.* **86**: 10, 1601–1609.

Smith, R. B. 1977. Formation of folds, boudinage and mullions in non-Newtonian materials. *Geol. Soc. Am. Bull.* **88**:2, 312–320.

Smith, R. B. 1979. The folding of a strongly non-Newtonian layer. *Am. J. Sci.* **279**: 3, 272–287.

Sowers, G. M. 1973. Theory of spacing of extension fracture. *Geol. Soc. Am. Bull.* Engineering case history No. 9.

Stephansson, O. & Berner, H. 1971. The finite element method in tectonic processes. *Phys. Earth & Planet Interiors* **4**, 301–321.

Strömgård, K. E. 1973. Stress distribution during deformation of boudinage and pressure shadows. *Tectonophysics* **16**, 215–248.

Summers, J. M. 1979. An experimental and theoretical investigation of multilayer fold development. Ph.D. thesis, University of London (unpublished).

Woldekidan, T. 1982. Deformation of multilayers compressed normal to the layering. Ph.D thesis, University of London (unpublished).